Japan Architectural Review
Open Access
Architectural Institute of Japan

Translated Paper

A new method for evaluating the real-time residual seismic capacity of existing structures using accelerometers: Structures with multiple degrees of freedom

Koichi Kusunoki,[1] Daiki Hinata,[2] Yuuki Hattori[3] and Akira Tasai[4]

[1]Earthquake Research Institute, The University of Tokyo, Tokyo, Japan; [2]Building Structures Group, Kajima Technical Research Institute, Tokyo, Japan; [3]Structural Design Department, Shimizu Corporation, Tokyo, Japan; [4]Department of Architecture and Building Science, Faculty of Urban Innovation, Yokohama National University, Yokohama, Japan

Correspondence
Koichi Kusunoki, Earthquake Research Institute, The University of Tokyo, Tokyo, Japan.
Email: kusunoki@eri.u-tokyo.ac.jp

Funding information
No funding information is provided.

The Japanese version of this paper was published in Volume 79, Number 699, pages 613-620, https://doi.org/10.3130/aijs.79.613 of *Journal of Structural Construction Engineering (Transactions of AIJ)*. The authors have obtained permission for secondary publication of the English version in another journal from the Editor of *Journal of Structural Construction Engineering (Transactions of AIJ)*. This paper is based on the translation of the Japanese version with some slight modifications.

Received July 7, 2017; Accepted October 5, 2017

doi: 10.1002/2475-8876.1010

Abstract

This paper presents a new method that involves the use of a double integral with a wavelet transform for computing the capacity curve of a system with multiple degrees of freedom. The displacement response of a building is derived from measurements of its acceleration, thus facilitating the assessment of the damage to the building as soon as possible after an earthquake. The validity of the method is assessed against existing shaking-table results for a reinforced concrete structure.

Keywords
acceleration, capacity curve, demand curve, residual seismic capacity, wavelet transform

1. Introduction

The Tohoku Earthquake that occurred on March 11, 2011 caused damage to buildings all over the northern part of Honshu, the main island of Japan. Several structural engineers who were supposed to conduct rapid inspections immediately after the earthquake encountered difficulties when carrying out their tasks. The earthquake revealed that even if local governments have arrangements in place to dispatch their structural engineers to support the rapid inspection of damage in neighboring prefectures that might be impossible if the earthquake damage is widespread. In the case of high-rise buildings, conducting a rapid inspection based on visual observation is unrealistic because it is time-consuming and subjective. Moreover, revisions made to the building code of Japan in 1981 encouraged the use of strong-column/weak-beam structural systems for absorbing more earthquake energy throughout the building, which thus makes it difficult to observe damage to hidden beams, such as those covered by ceilings. Furthermore, given that all the beams in the building are required to be inspected, visual inspection is clearly impractical.

Recently, much research has been conducted on the methods for monitoring building structural health aimed at evaluating damage,[1-8] with system identification being one such method.[1-4] However, although the target structure and/or the number of sensors differed, the major part of this research was based on detecting damage via changes in the predominant period or story stiffness of the structure. Other studies have been focused on deriving physical values such as the story stiffness using measured signals.[5,6] However, such an approach requires engineering judgment in order to evaluate the damage level because the relationship between story stiffness degradation and building damage is strongly dependent on the structural type and shape. Nakamura and Yasui[7] compared the actual damage to a steel structure using values estimated using measurements and then proposed criteria for relating the story stiffness degradation to the story damage. Kurata et al[8] proposed a method for predicting damage locations from changes in vibration characteristics based on the pre-learned relationship between the vibration characteristics and damage patterns.

As a distinct alternative approach, Kusunoki et al proposed a new real-time system for evaluating the residual seismic capacity using inexpensive accelerometers placed at each story.[9-11] This system allows the level of damage to a building to be communicated to its owners and residents immediately after an earthquake. It is relatively easy to implement because the building in question need only be instrumented with in situ sensors and a server and need not be modeled on a computer.

1.1 Outline of evaluation method

The schematic of the proposed evaluation method is shown in Figure 1. The maximum responses during the main shock and aftershock are estimated from the intersection of the capacity and demand curves. The capacity curve is the relationship between the representative restoring force and representative displacement, which are derived from the measured accelerations. The demand curve represents the relationship between the response acceleration spectrum and response displacement spectrum, which are derived from the acceleration at the basement of the building. In order to derive the demand curve, a value has to be assigned to the damping coefficient. During the elastic stage, the damping coefficient can be considered as a viscous damping ratio of 5%, as shown in curve 1 in Figure 1. After the building has undergone yielding at point A in Figure 1, an additional damping effect is required because of the nonlinear response thus induced. Because this additional damping effect increases according to the amount of damage to the building, the total damping coefficient increases according to the representative displacement. Therefore, the demand curve is reduced from point B, as shown in curve 2 in Figure 1. The maximum response during the main shock is predicted from the intersection at point C of the capacity curve and the reduced demand curve (curve 2).

The same method can be used to predict the maximum response during an aftershock by considering the main shock and its subsequent aftershock as a single earthquake of a very long duration. Given that the input energy of the combined earthquake is greater than that of the main shock alone, the maximum response of the former should also be greater. This means that the equivalent damping effect is less than that of the main shock alone, as indicated by curve 3 in Figure 1. The predicted maximum response during the aftershock is the intersection of curve 3 and the capacity curve, assuming that the maximum response of the aftershock is the same as that of the main shock.

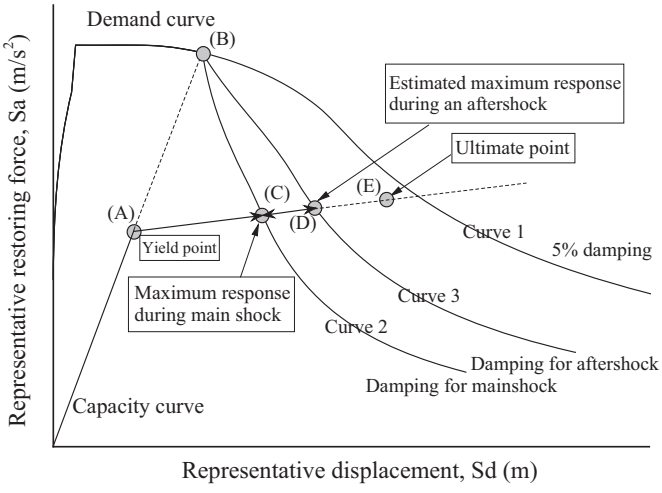

Figure 1. Outline of evaluation method

In order to determine the safety of the building, the first mode of its response must be extracted to derive the capacity curve. The ultimate point is defined according to the safety limit of each story. The maximum story drift of each story is derived from the maximum representative displacement and the shape of the first mode. Because the proposed safety evaluation is based on the first mode, the effects of higher order modes should be considered separately, unless such effects are negligible as in the case of a high-rise building.

1.2 Objectives

In order to evaluate the residual seismic capacity of a building, its capacity curve must be derived accurately. This accuracy depends on that of the displacement, which is obtained from a double integration of the measured acceleration. Kusunoki and Teshigawara proposed a method for performing a double integration of the measured acceleration in the temporal domain, by considering the predominant period of the building, which allowed them to obtain the capacity curve of a multiple degrees-of-freedom (MDOF) system.[9] However, their proposed method involves the assumption that the building vibrates only in its first mode (see the appendix of Ref. 9), and thus, it cannot consider the effects of higher order modes; furthermore, no change in equivalent mass owing to nonlinear response can be considered.

In contrast, using a wavelet transform (WT) to perform the double integration could result in a more realistic displacement because the WT would decompose the first mode vibration.[12] Changes in the equivalent mass due to nonlinearity could also be taken into consideration. The aims of the present study were to extend the method proposed in Ref. 10 to an MDOF system and to assess the validity of the extended method against the results of shaking-table tests. Moreover, a tri-linear method for modeling the capacity curve is proposed for evaluating the level of damage in a building.

2. Method for simplifying an MDOF system to an single degree-of-freedom (SDOF) system

In this section, a method is introduced for simplifying an MDOF system to an SDOF system; this is effectively equivalent to a linearization method.[13–18] In practice, the restoring force and the displacement response relative to the basement are obtained via static nonlinear analysis (pushover analysis).

The equation of motion for the MDOF system is

$$[M]\{\ddot{x}\} + [C]\{\dot{x}\} + [K]\{x\} = -[M]\{1\}\ddot{x}_0, \tag{1}$$

where $[M]$ is the mass matrix, $[C]$ is the damping matrix, $[K]$ is the stiffness matrix, $\{\ddot{x}\}$ is the acceleration vector relative to the basement, $\{\dot{x}\}$ is the velocity vector relative to the basement, $\{x\}$ is the displacement vector relative to the basement, and $\ddot{x}_0$ is the ground acceleration.

A system with N degrees of freedom has N predominant periods and predominant modes. By solving the eigenvalue equation, we obtain an eigenperiod ${}_sT$, an angular eigenfrequency ${}_s\omega(=2\pi/{}_sT)$, and an eigenmode vector $\{{}_su\}$ for the sth mode. The relative displacement vector {x} is derived as follows from the response of each mode:

$$\{x\} = \sum_{s=1}^{N} \{{}_su\} \cdot {}_sq = [U]\{q\}, \tag{2}$$

where ${}_sq$ is the response displacement of the sth mode.

By substituting Equation (2) into Equation (1), N equations are obtained for ${}_sq$:

$$ {}_s\ddot{q} + 2{}_sh \cdot {}_s\omega \cdot {}_s\dot{q} + {}_s\omega^2 \cdot {}_sq = -{}_s\beta \cdot \ddot{x}_0, \quad (3) $$

$$ s = 1, 2, \ldots, N, $$

$$ {}_s\beta = \frac{\{{}_su\}^T[M]\{1\}}{\{{}_su\}^T[M]\{{}_su\}} = \frac{\sum m_i \cdot {}_su_i}{\sum m_i \cdot {}_su_i^2}, $$

where ${}_sh$ is the damping coefficient for the sth mode, ${}_s\beta$ is its stimulation factor, and ${}_s\beta\cdot\{{}_su\}$ is its stimulation vector, which is the eigenmode for the sth mode of the unit vector $\{1\}$:

$$ \{1\} = \sum_{s=1}^{N} {}_s\beta \cdot \{{}_su\}. \quad (4) $$

The response of each mode can be calculated as the response for the same ground acceleration of $\ddot{x}_0$ with ${}_sq_0$:

$$ {}_sq = {}_s\beta \cdot {}_sq_0. \quad (5) $$

Based on Equation (5), Equations (6) and (7) are derived from Equations (2) and (3), respectively:

$$ \{x\} = \sum_{s=1}^{N} {}_s\beta \cdot \{{}_su\} \cdot {}_sq_0, \quad (6) $$

$$ {}_s\ddot{q}_0 + 2{}_sh \cdot {}_s\omega \cdot {}_s\dot{q}_0 + {}_s\omega^2 \cdot {}_sq_0 = -\ddot{x}_0, \quad (7) $$

$$ s = 1, 2, \ldots, N. $$

The base shear ${}_sQ_B$ of the sth mode is obtained as shown in Equation (8), by assuming that the shape of the external force distribution is proportional to the mode shape:

$$ {}_sQ_B = {}_s\bar{M} \cdot ({}_s\ddot{\Delta} + \ddot{x}_0) = \sum_{i=1}^{N} m_i \cdot {}_s\beta \cdot {}_su_i({}_s\ddot{\Delta} + \ddot{x}_0), \quad (8) $$

where ${}_s\ddot{\Delta}$ is the relative representative acceleration for the sth mode. The equivalent mass ${}_s\bar{M}$ for the sth mode is obtained as

$$ {}_s\bar{M} = \frac{(\sum m_i \cdot {}_su_i)^2}{\sum m_i \cdot {}_su_i^2}. \quad (9) $$

The displacement relative to the basement for the sth mode is obtained as shown in Equation (10) with the stimulation vector and the representative displacement:

$$ \{{}_sx\} = {}_s\beta \cdot \{{}_su\} \cdot {}_s\Delta, \quad (10) $$

where ${}_s\Delta$ is the representative displacement for the sth mode. From Equation (10), we obtain

$$ \sum m_i \cdot {}_su_i = \frac{1}{{}_s\beta \cdot {}_s\Delta} \sum m_i \cdot {}_sx_i, \quad (11) $$

$$ \sum m_i \cdot {}_su_i^2 = \left(\frac{1}{{}_s\beta \cdot {}_s\Delta}\right)^2 \sum m_i \cdot {}_sx_i^2. \quad (12) $$

Equation (13) is obtained from Equation (9) by using Equations (11) and (12):

$$ {}_s\bar{M} = \frac{(\sum m_i \cdot {}_sx_i)^2}{\sum m_i \cdot {}_sx_i^2}. \quad (13) $$

The representative acceleration is derived from Equation (8), as shown in Equation (14), for an external lateral force ${}_sP_i$ and relative displacement ${}_sx_i$ obtained from a pushover analysis, with the shape of the lateral force distribution being that of the sth mode:

$$ ({}_s\ddot{\Delta} + \ddot{x}_0) = \frac{{}_sQ_B}{{}_s\bar{M}} = \frac{\sum m_i \cdot {}_sx_i^2}{(\sum m_i \cdot {}_sx_i)^2} \cdot \sum_{i=1}^{N} {}_sP_i. \quad (14) $$

Furthermore, from Equation (10), we obtain

$$ {}_s\beta \cdot \{{}_su\} = \frac{1}{{}_s\Delta}\{{}_sx\}, \quad (15) $$

and from Equations (8), (13), and (15), we obtain

$$ {}_s\bar{M} = \frac{\sum_{i=1}^{N} m_i \cdot \frac{{}_sx_i}{{}_s\Delta}({}_s\ddot{\Delta} + \ddot{x}_0)}{{}_s\ddot{\Delta} + \ddot{x}_0} = \frac{(\sum m_i \cdot {}_sx_i)^2}{\sum m_i \cdot {}_sx_i^2}. \quad (16) $$

Therefore, the representative displacement ${}_s\Delta$ is obtained from Equation (16) as

$$ {}_s\Delta = \frac{\sum m_i \cdot {}_sx_i^2}{\sum m_i \cdot {}_sx_i}. \quad (17) $$

As the calculated values of ${}_s\ddot{\Delta}$ and ${}_s\Delta$ in Equation (7) are ${}_s\ddot{q}_0$ and ${}_sq_0$, respectively, the relationship between ${}_s\ddot{\Delta}$ and ${}_s\Delta$ is given by Equation (18) where the sth angular eigenfrequency is ${}_s\omega$:

$$ {}_s\ddot{\Delta} + \ddot{x}_0 \approx {}_s\omega^2 \cdot {}_s\Delta. \quad (18) $$

When a building is in an elastic state, the maximum values of $|{}_s\ddot{\Delta} + \ddot{x}_0|$ and $|{}_s\Delta|$ are the same as those of the response spectra of S_a and S_d, respectively, for an adequate damping coefficient. The curve of the relationship between $|{}_s\ddot{\Delta} + \ddot{x}_0|$ and $|{}_s\Delta|$ is defined as the capacity curve. The gradient of the capacity curve at its origin is the square of the equivalent angular frequency in the nonlinear range, ie, ω^2, and the same is true of the demand curve (ie, the relationship between S_a and S_d). The intersection of the performance and demand curves has the same equivalent angular frequency as that in Equation (18).

3. Capacity curve obtained from measured accelerations

The method for calculating the capacity curve (ie, the relation between representative acceleration ${}_1\ddot{\Delta} + \ddot{x}_0$ and representative displacement ${}_1\Delta$) from the acceleration measured at each story is introduced in this section. The displacement of each story is obtained from a double integration of the measured accelerations as in Ref. 10 The first mode is obtained by using a WT to extract the predominant vibration from the measured response.

3.1 Outline of wavelet transform

A WT is a time-frequency analysis method for mathematically assessing the degree of similarity between a signal $f(x)$ and a mother wavelet.[19] An original signal f_0 is decomposed into g_1, which is a component with a particular frequency band, and a residual f_1:

$$ f_0 = g_1 + f_1. \quad (19) $$

By repeating this procedure, the original signal is decomposed as

$$ f_0 = g_1 + g_2 + g_3 + \cdots + g_n + f_n, \quad (20) $$

where the signal g_i of the ith decomposition is referred to as the signal of rank i (ie, the ith rank). The maximum

rank n corresponds to the number N of decomposed signals:

$$n = \log_2 N. \tag{21}$$

where f_n is a deterministic value; the orthogonality of the decomposed signals has been proved mathematically.

A WT can be considered as a time-frequency analysis windowed by the mother wavelet. The widths Δ_t and Δ_f of the window in the temporal and frequency domains, respectively, are related through the following uncertainty relationship:

$$2\Delta_t \cdot 2\Delta_f \geq 2. \tag{22}$$

If the time increment of the original signal $f(x)$ is Δ_t, then that of g_i, ie, $\Delta_{t,i}$, is

$$\Delta_{t,i} = \Delta_t \times 2^i. \tag{23}$$

The Nyquist frequency $\Delta_{f,i}$ of the rank i signal g_i is

$$\Delta_{f,i} = \frac{1}{2\Delta_t \cdot 2^i}. \tag{24}$$

Hence, the WT satisfies the minimum uncertainty relationship shown in Equation (22).

In order to obtain the displacement from the measured acceleration using conventional filtering techniques such as a bandpass filter,[9] an appropriate baseline shift correction must be applied and a filtering frequency must be defined; however, there is as yet no general method for this. In contrast, a WT can decompose any type of signal in the temporal domain and can extract any mode from the decomposed ranks based on its frequency.

3.2 Capacity curve from wavelet transform

The objectives of applying a WT to the measured acceleration are to obtain a reasonable response displacement while eliminating errors in the measured acceleration and to extract the predominant mode from the measured response.[10] The first mode can be extracted from the measured response using the WT by considering the ranks of those frequency bands that contain the predominant frequency of the building[20]; such ranks are referred to here as "predominant ranks" and are discussed in detail in Section 5.2.

The measured acceleration and the acceleration for each rank are schematically presented in Figure 2, where $\ddot{X}_i$ is the absolute acceleration at floor i, $\ddot{x}_i$ is the relative acceleration at floor i, $\ddot{x}_0$ is the ground acceleration, ${}_1\ddot{x}_i$ is the relative acceleration for the first mode at floor i, and ${}_1\ddot{x}_0$ is the first mode component of the ground acceleration.

The quantities ${}_1\ddot{x}_0$ and ${}_1\ddot{x}_0 + {}_1\ddot{x}_i$ can respectively be obtained by applying WTs to the ground acceleration $\ddot{x}_0$ and measured absolute acceleration $\{\ddot{X}\}$. The displacement relative to the basement is obtained by performing a double integration of the measured acceleration:

$${}_1x_i = \int\int ({}_1\ddot{x}_0 + {}_1\ddot{x}_i)dt^2 - \int\int {}_1\ddot{x}_0 dt^2. \tag{25}$$

Because the relative displacement and acceleration obtained using WTs do not comprise appreciable higher mode components, they are assumed to be the first-mode responses.

3.3 Capacity curve from measured acceleration

It was shown in Section 2 that the representative acceleration ${}_s\ddot{\Delta} + \ddot{x}_0$ and representative displacement ${}_s\Delta$ can be derived using Equations (14) and (17), respectively, in a practical structural design. Because the method proposed here is based on the first mode, Equations (26) and (27) are obtained from Equations (14) and (17), respectively:

$$({}_1\ddot{\Delta} + {}_1\ddot{x}_0) = \frac{\sum m_i \cdot {}_1x_i^2}{(\sum m_i \cdot {}_1x_i)^2} \cdot \sum_{i=1}^{N} {}_1P_i, \tag{26}$$

$${}_1\Delta = \frac{\sum m_i \cdot {}_1x_i^2}{\sum m_i \cdot {}_1x_i}. \tag{27}$$

The representative displacement can be obtained from Equation (27) by using the relative displacement obtained from Equation (25).

The shape of the external force distribution ${}_1P$ of Equation (26) should be proportional to the first mode vector. As shown in Figure 2b, the ground acceleration contributes a constant factor ${}_1\ddot{x}_0$ to the acceleration at each story. However, the

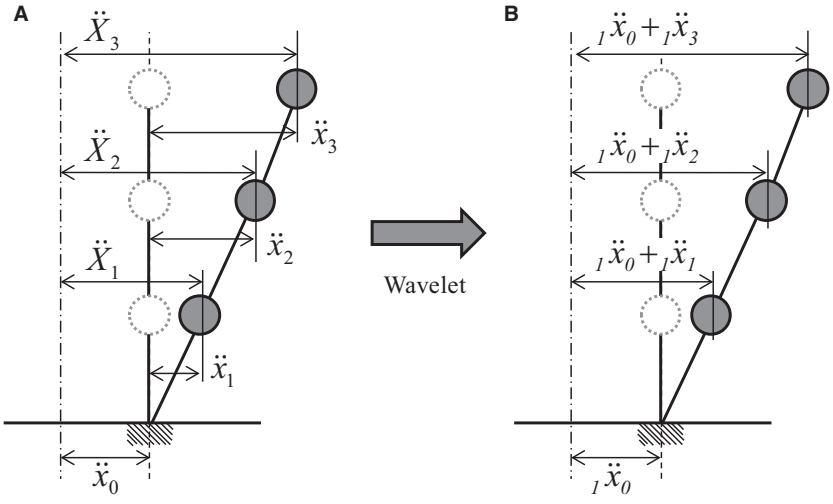

Figure 2. Schematics of (a) measured acceleration and (b) acceleration for each rank obtained using wavelet transform

distribution of the relative acceleration ${}_1\ddot{x}_i$ obtained by using the WT is proportional to the first mode vector. As a result, the distribution of the absolute acceleration ${}_1\ddot{x}_0 + {}_1\ddot{x}_i$ is not proportional to the first mode vector. In order for the absolute acceleration to be proportional to the first mode vector, the stimulation factor ${}_1\beta \cdot \{{}_1u\}$ of the first mode must be multiplied by the ground acceleration ${}_1\ddot{x}_0$. This means that the first mode of the unit vector $\{1\}$ is multiplied by the ground acceleration. As a result, the external force proportional to the first mode vector is obtained as

$$ {}_1P_i = m_i({}_1\ddot{x}_i + {}_1\beta \cdot {}_1u_i \cdot {}_1\ddot{x}_0). \tag{28} $$

The representative acceleration in Equation (29) is obtained by substituting Equation (28) into Equation (26):

$$ \begin{aligned} ({}_1\ddot{\Delta} + {}_1\ddot{x}_0) &= \frac{\sum m_i \cdot {}_1x_i^2}{(\sum m_i \cdot {}_1x_i)^2} \cdot \sum_{i=1}^{N} (m_i \cdot {}_1\ddot{x}_i + m_i \cdot {}_1\beta \cdot {}_1u_i \cdot {}_1\ddot{x}_0) \\ &= \frac{\sum m_i \cdot {}_1x_i^2}{(\sum m_i \cdot {}_1x_i)^2} \sum_{i=1}^{N} m_i \cdot {}_1\ddot{x}_i + {}_1\ddot{x}_0. \end{aligned} \tag{29} $$

As shown in Equation (29), only the relative acceleration term of the representative acceleration is required to be divided by the equivalent mass ratio when the representative acceleration is derived from the measured accelerations.

In Equations (27) and (29), the order of the mass m_i is the same in the denominator and the numerator. Therefore, we require the mass ratio between floors instead of the absolute mass. If the usage of the building is the same for all floors, the floor-area ratio can be used instead of the mass ratio.

However, Equations (27) and (29) do not provide a practical capacity curve if the response displacement is very small. As an example, Figure 3 shows the capacity curve derived using Equations (27) and (29) for the results of shaking-table tests on a 3-story full-scale reinforced concrete (RC) specimen, the details of which are described in Section 5.1. As shown in Figure 3, the representative acceleration thus obtained was extremely large over a relatively small range of representative displacement. This is because the distribution of the calculated relative displacement at each floor was not proportional to the first mode vector owing to errors in the measured values at small displacements that caused the equivalent mass ratio to become excessively small.

The distribution shape was not proportional to the first mode vector because of small errors in the measured acceleration that were not eliminated perfectly by the WT and that were subsequently amplified by the double integral. The error components exist throughout the measured acceleration, but their effects become more pronounced as the actual displacement decreases. In order to avoid the effects of these errors, firstly a "tentative" representative displacement ${}_1\Delta'$ and a "tentative" representative acceleration ${}_1\ddot{\Delta}' + {}_1\ddot{x}_0$ are calculated using Equations (30) and (31), respectively, and a "tentative" capacity curve can be obtained from the relationship between them:

$$ {}_1\Delta' = {}_1\Delta \cdot \frac{{}_1\bar{M}}{M} = \frac{\sum m_i \cdot {}_1x_i}{\sum m_i}, \tag{30} $$

$$ ({}_1\ddot{\Delta}' + {}_1\ddot{x}_0) = \left({}_1\ddot{\Delta} \cdot \frac{{}_1\bar{M}}{M} + {}_1\ddot{x}_0 \right) = \frac{\sum m_i \cdot {}_1\ddot{x}_i}{\sum m_i} + {}_1\ddot{x}_0. \tag{31} $$

These 2 equations are obtained by dividing Equation (27) and the first term of Equation (29) by the equivalent mass ratio (ie, the ratio of the equivalent mass to the total mass). Because the equivalent mass ratio is not used in Equations (30) and (31), the error shown in Figure 3 no longer arises in the case of small displacements. However, the slope of the tentative capacity curve does not coincide with the predominant frequency.

The procedure for calculating the capacity curve from the tentative capacity curve is as follows:

1. A tentative capacity curve is derived from the mass ratio and measured acceleration.
2. The tentative capacity is then used to produce a backbone curve, which is a curve consisting of the points at which the maximum tentative representative displacement is updated in the positive direction and the minimum tentative representative displacement is updated in the negative direction.[9]
3. The equivalent mass ratio is calculated for the points of the backbone curve, whereupon the capacity curve is calculated by dividing the tentative representative displacement and the first term of the tentative representative acceleration by the equivalent mass ratio.

3.4 Demand curve with measured acceleration

The demand curve, which is compared with the capacity curve for predicting the maximum response, is calculated using the

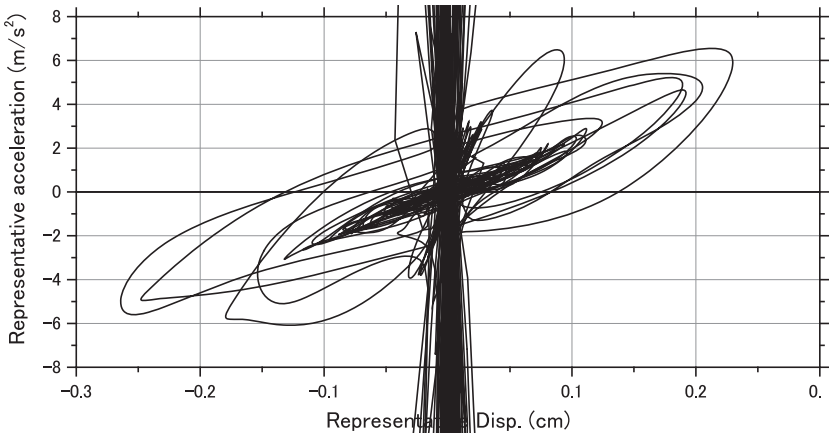

Figure 3. Example of capacity curve derived from measured accelerations

ground acceleration $\ddot{x}_0$ as measured at the basement of the building. The ground acceleration ${}_1\ddot{x}_0$ for the capacity curve is the first mode component of the ground acceleration that is extracted by the WT. Therefore, the ground accelerations for the demand curve and capacity curve are different. Because ${}_1\ddot{x}_0$ is extracted from $\ddot{x}_0$ as the predominant component that affects the response of the building, the demands for the predominant period of the building from the demand curves that are calculated using $\ddot{x}_0$ and ${}_1\ddot{x}_0$ are almost the same.

Figure 4 shows the calculated demand curves with the measured ground acceleration $\ddot{x}_0$ during the shaking-table tests (the details of which are described in Section 5), which are indicated as "Original," and with the component ${}_1\ddot{x}_0$ of the predominant ranks shown as "Rank 6 + 7 + 8 + 9." The Nyquist frequencies of ranks 5-8 are also superimposed on the figure. Figure 4 shows that both demand curves coincide very well in the predominant frequency band of ranks 5-8. However, outside the predominant frequency band, especially for periods less than 0.32 s (rank 5), the difference between demand curves is significant. Because a period of less than 0.32 s is much shorter than the predominant period of the specimen, it has no effect on the evaluation of the maximum response. Therefore, the demand curve can be calculated using the acceleration $\ddot{x}_0$ measured at the basement.

3.5 Modeling the capacity curve

In order to evaluate the residual seismic capacity of the building, the capacity curve is required to be modeled using 4 straight lines (quad-linear model) while considering the negative slope proposed in Ref. 10. We describe here the method for calculating the restoring force and displacement at each corner point, but the details are available in Ref. 10. The schematic of the modeling process is shown in Figure 5, and the procedures are as follows, where (δ_c, F_c), (δ_y, F_y), ($\delta_{F_{max}}$, F_{max}), and (δ_u, F_u) are the displacement and restoring force at the first, second, third, and fourth corner points, respectively:

1. The initial stiffness is the slope between the origin and the point at which the restoring force is 1/4 of F_{max} and F_c is 1/3 of F_y.
2. The second corner point is defined such that the slope between (δ_y, F_y) and ($\delta_{F_{max}}$, F_{max}) is 1/1000 of the initial stiffness and the dissipated strain energies from the origin to ($\delta_{F_{max}}$, F_{max}) of the capacity curve and the model are the same.
3. The point at which the restoring force is maximum is the third corner point.
4. The measured maximum displacement is δ_u, and F_u is defined such that the dissipated strain energies from the origin to (δ_u, F_u) of the capacity curve and the model are the same.

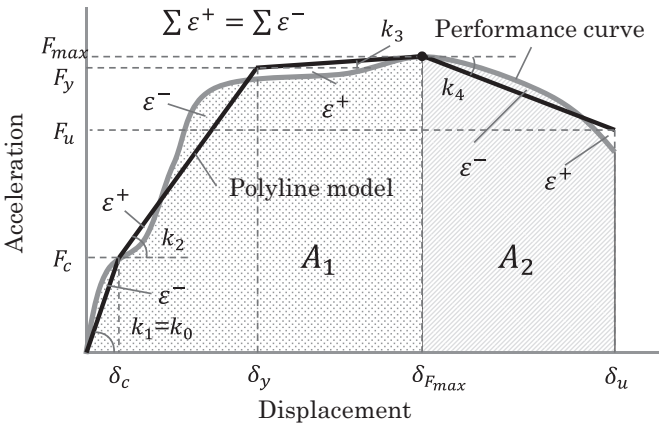

Figure 5. Schematic of modeling process

If ($\delta_{F_{max}}$, F_{max}) and (δ_u, F_u) are the same point, the capacity curve is modeled as a tri-linear model.

4. Evaluation of method for obtaining capacity curve using dynamic analysis

In this section, the slope of the capacity curve obtained using the method introduced in Section 3 is compared with the predominant angular frequency for assessing the accuracy of the method. In order to compare the capacity and demand curves, the slope of the capacity curve is required to be equal to the square of the predominant angular frequency. A dynamic linear analysis, in which the predominant angular frequency is known, is conducted in this section. The capacity curve in the nonlinear range is discussed in Section 5.

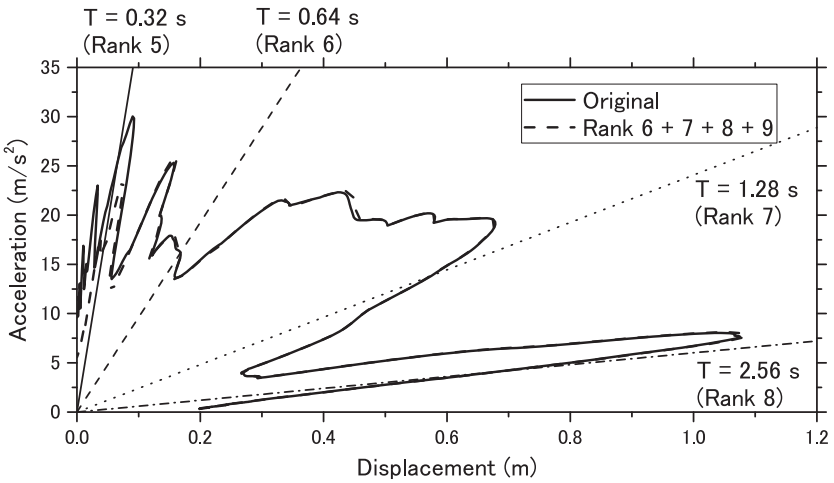

Figure 4. Demand curves with $\ddot{x}_0$ and ${}_1\ddot{x}_0$

Table 1. Parameters of analysis

Story	Mass	Stiffness
1F	490 kN	147 kN/cm
2F	490 kN	29.4 kN/cm

Table 2. Results of eigenvalue analysis

	1st mode	2nd mode
Eigenvalue		
1F	0.22	0.78
2F	1.15	−0.15
Predominant period	0.91 s	0.33 s
Equivalent mass ratio	0.69	0.31

4.1 Outline of analysis

The north-south (NS) component of the acceleration recorded in Sendai City at station MYG013 of the K-NET system during the 2011 Tohoku Earthquake is applied as the input motion. The model is a linear system with 2 degrees of freedom and an equivalent mass ratio that is sufficiently small that the effect of the second mode is not negligible. The time increment in the analysis is 0.01 s, and the damping effect is modeled such that it is proportional to the stiffness with a coefficient of 3%. The mass and stiffness for each story are listed in Table 1. Table 2 presents the eigenvalue, predominant period, and equivalent mass ratio for each mode.

One of the aims of this analysis was to confirm the ability of the WT to extract the first mode accurately even if the effect of the second mode is not negligible.

4.2 Capacity curve obtained using analysis

Figure 6 shows the capacity curve derived with Equations (27) and (29) from the first mode extracted in the dynamic analysis, superimposed with the straight line whose slope is calculated from the first mode period. The figure clearly shows that the slope of the capacity curve coincides well with its predominant period.

Based on these results, we conclude that the calculation method for the capacity curve proposed in Section 3.3 is valid and that the WT can be used for extracting the first mode efficiently from the response.

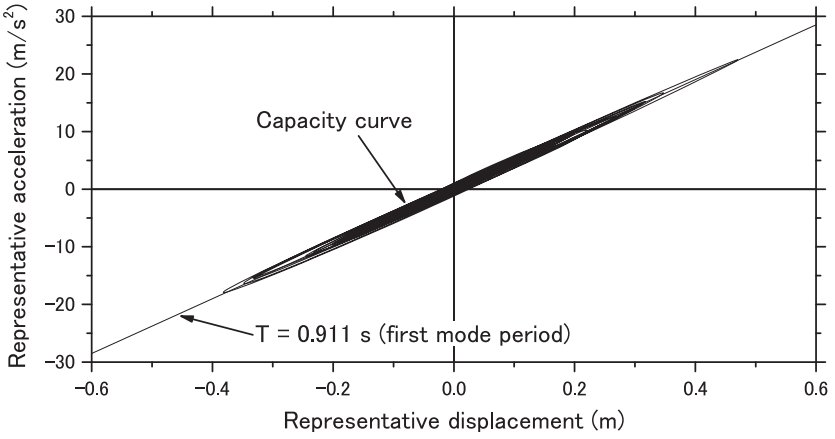

Figure 6. Capacity curve (dynamic analysis)

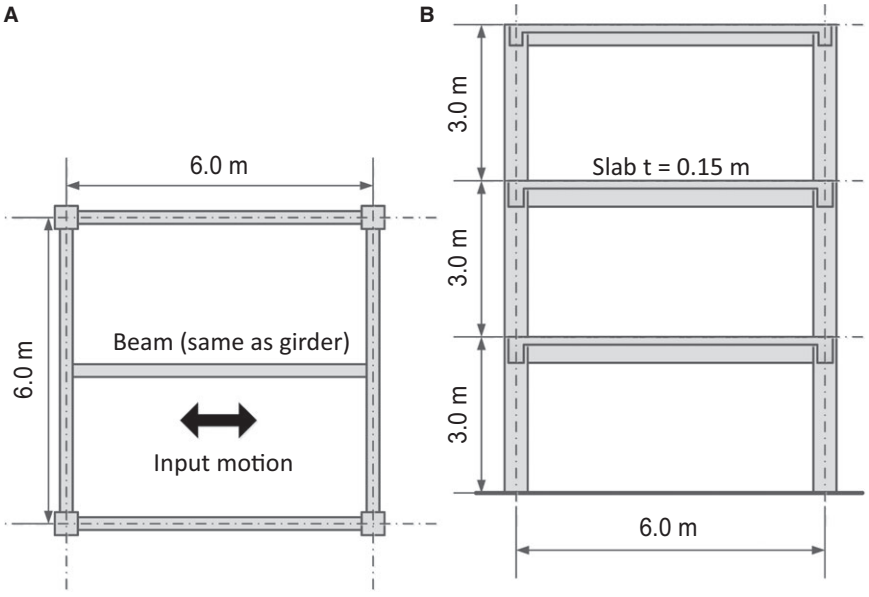

Figure 7. Dimensions of test specimen (see Refs. 21-25): (a) plan view; (b) elevation

Table 3. Outline of the test specimen (see Refs. 21-25)

	Column	Beam (RF)	Beam (1,2F)
Dimensions (mm)	450 × 450	250 × 400	300 × 500
Rebar			
Upper	8-D22	2-D22	2-D22 + 1-D19
Lower		2-D16	2-D22
Hoop	D10 with spacing of 100	D10 with spacing of 200	D10 with spacing of 200
F_c (kgf/cm^2)	300		

5. Capacity curve obtained from measured acceleration

In this section, the validity of the proposed method for calculating the capacity curve is assessed against acceleration records measured during shaking-table tests performed in a 1-span/1-bay 3-story RC specimen.[21-25]

5.1 Outline of test specimen

The test specimen was a 1-span/1-bay 3-story RC specimen that was tested in 1993 at the National Research Institute for Earth Science and Disaster Resilience (NIED) in Japan. An outline of the shaking-table tests is given here, but the details can be found in the associated references.[21-25] The dimensions of the specimen are shown in Figure 7, and its specifications are outlined in Table 3.

The input motion is the east-west component of the Hachinohe record, of which the peak ground acceleration was amplified to 600 cm/s^2. The accelerometers (Kyowa AS-5GB, dynamic strain type) were placed at the center of each floor and were sampled at a rate of 200 Hz. Yield hinges formed at

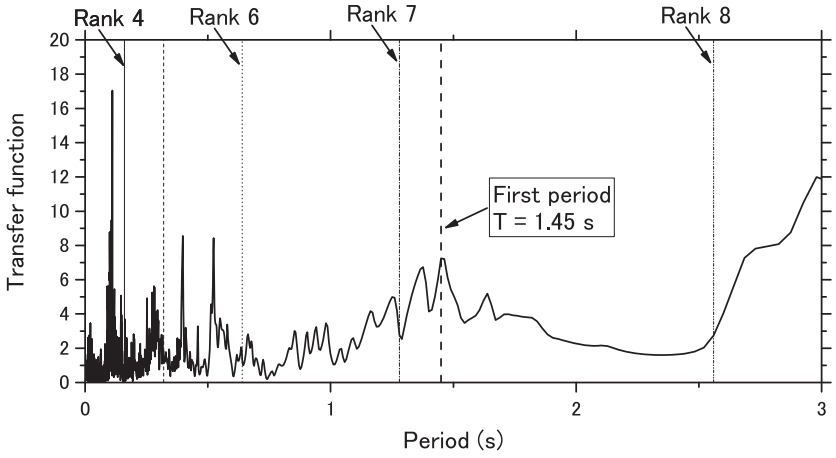

Figure 8. Transfer function

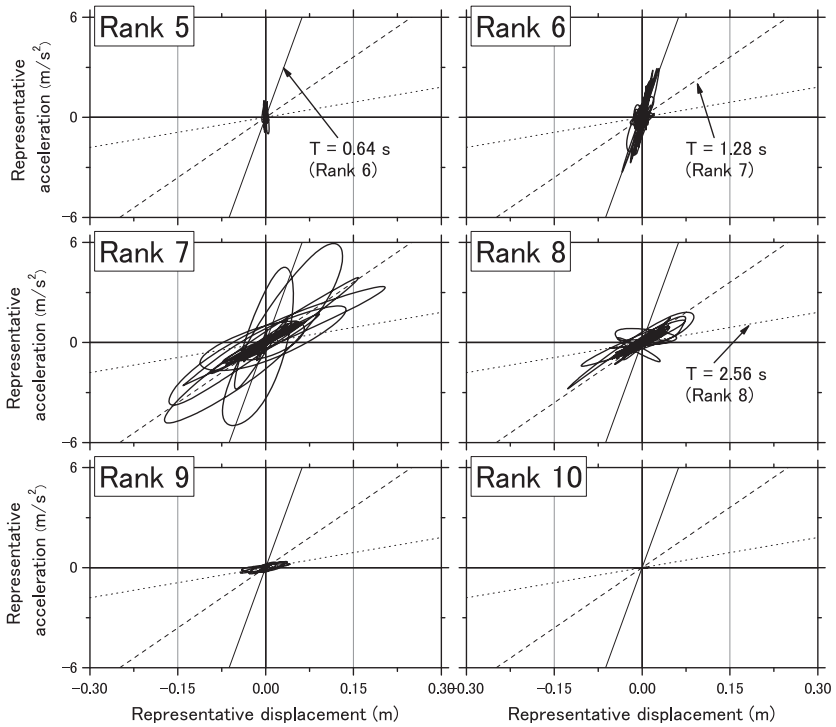

Figure 9. Capacity curve for each rank

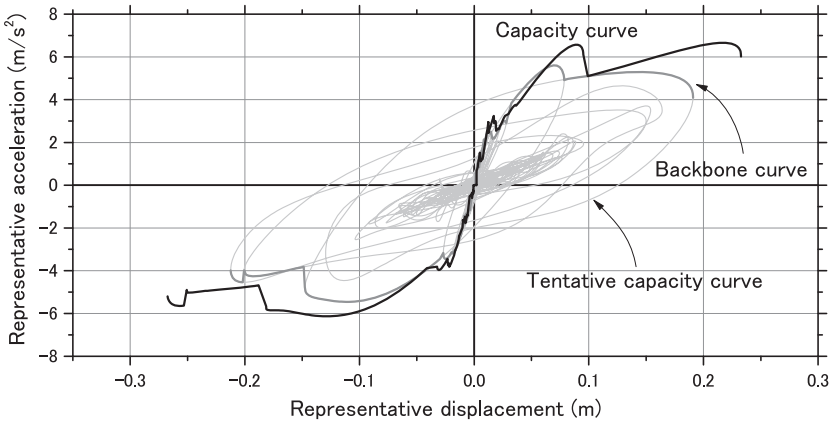

Figure 10. Capacity curve

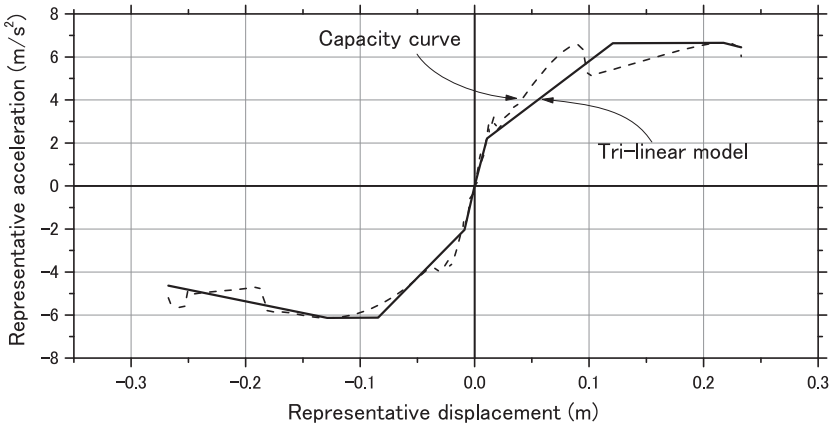

Figure 11. Capacity curve and tri-linear model

either end of every beam and at the bottom of the columns of the first floor.[21-25]

5.2 Selection of predominant rank

The predominant rank is selected by predicting the predominant frequency band based on the transfer function and comparing the tentative capacity curves of the ranks in the frequency band and their slopes. The transfer function from the bottom to the top of the specimen is shown in Figure 8. The tentative capacity curves of ranks 5-10 are shown in Figure 9. The Nyquist frequencies for those ranks are also indicated using dashed lines in both figures.

It can be seen from Figure 8 that there is a peak at a period of 1.45 s, and that the predominant period of the specimen is between ranks 7 and 8. Figure 9 shows the tentative capacity curves for ranks 6-8, which show a strong correlation. The tentative capacity curve for rank 9 shows that the structure oscillates at the same period as that of rank 8. In contrast, the tentative capacity curves for ranks 5 and 10 show very small responses, and the predominant periods are quite different from those for ranks 6-9. Therefore, the predominant ranks are considered to be ranks 6-9.

5.3 Capacity curve derived from measured accelerations

The capacity curves for the predominant ranks selected in Section 5.2 are derived in this section. The derived capacity curve, tentative capacity curve, and backbone curve are shown in Figure 10. The tri-linear model derived as described in Section 3.5 is shown in Figure 11, where the capacity curve is indicated by the dashed line. The tri-linear model represents the capacity curve well. Hence, it is confirmed that the capacity curve for evaluating the residual seismic capacity of an existing building can be derived only from the measured accelerations.

6. Concluding remarks

In this paper, an existing method for calculating the capacity curve of an actual building from measured accelerations of an SDOF system was extended to an MDOF system. The extended method was verified using linear dynamic analysis and the results from shaking-table tests. The findings of this research are listed below:

1. A method was proposed for calculating the capacity curve of a multi-story building, and the capacity curve thus derived was shown to be comparable with the demand curve.
2. The validity of the proposed method was confirmed using linear dynamic analysis by comparing the predominant period.
3. The results of shaking-table tests confirmed that the capacity curve could be derived from measured accelerations processed with WTs, and that the proposed modeling method produced a reasonable tri-linear model.

Acknowledgments

The authors thank Prof. Kenji KITAJIMA of Nihon University for kindly providing the data for the full-scale 3-story RC shaking-table tests. The authors also thank K-NET of NIED for kindly allowing us to use the recorded earthquake data.

Disclosure

The authors have no conflict of interest to declare.

References

1 Saito T. Probabilistic damage estimation through structural identification. *J Struct Constr Eng*. 2002;**557**:93-100 (in Japanese).
2 Hamamoto T, Morita K, Teshigawara M. Story damage detection of multistory building using natural frequency shifts of multiple modes. *J Struct Constr Eng*. 2002;**67**:93-100 (in Japanese).
3 Hamamoto T, Oeki Y, Miyoshi T. Damage detection of multistory buildings using active identification scheme. *J Struct Constr Eng*. 2001;**66**:51-56 (in Japanese).
4 Hamamoto T, Kondo I. Two-stage damage detection of eccentric multistory buildings using vertical and horizontal searching. *J Struct Constr Eng*. 1999;**64**:21-28 (in Japanese).
5 Nitta Y, Nishitani A. Structural health monitoring of story stiffness based on identification of subsystem representing specific story of a building. *J Struct Constr Eng*. 2003;**68**:75-79 (in Japanese).
6 Nakamura M, Takewaki I, Yasui Y, Uetani K. Simultaneous identification of stiffness and damping of building structures using limited earthquake records. *J Struct Constr Eng*. 2000;**65**:75-82 (in Japanese).
7 Nakamura M, Yasui Y. Damage evaluation of a steel structures subjected to strong earthquake motion based on ambient vibration measurement. *J Struct Constr Eng*. 1999;**64**:61-68 (in Japanese).
8 Mayako Y, Masahiro K, Masayoshi N. Development of damage detection system for steel structures using data-mining. AIJ Kinki Chapter research meeting. Structure (52), 93-96, 2012 (in Japanese)
9 Kusunoki K, Teshigawara M. A new acceleration integration method to develop a real-time residual seismic capacity evaluation system. *J Struct Constr Eng*. 2003;**68**:119-126 (in Japanese).
10 Kawamura M, Kusunoki K, Yamashita M, Hattori Y, Hinata D, Diaz Figueroa MA, Tasai A. Study of a new method to compute the performance curve of real structures with acceleration sensors, in the case of SDOF system structures. *J Struct Constr Eng*. 2013;**78**:1061-1069 (in Japanese).
11 Kusunoki K, Teshigawara M. Numerical study for estimating the substitute damping coefficient for an aftershock. *Proc Jpn Concr Inst*. 2006;**28**:1057-1062 (in Japanese).
12 Matsumoto H, Maeda R, Kusunoki K, Tasai A. An experimental study on the validity of the wavelet transform to calculate performance curve. *Proc Jpn Concr Inst*. 2009;**31**:895-900 (in Japanese).
13 Akane J, Matsumoto H, Kusunoki K, Tasai A. A study on accuracy of performance curve from measured accelerations with sensors. *Proc Jpn Concr Inst*. 2007;**29**:1039-1044 (in Japanese).
14 Isaji K, Maeda R, Kusunoki K, Tasai A. An analytical study to evaluate equivalent period and damping coefficient for residual seismic capacity evaluation system with wavelet transformation. *Proc Jpn Concr Inst*. 2010;**32**:925-930 (in Japanese).
15 Kuramoto H, Teshigawara M, Koshiika N, Isoda H. Conversion of multistory building into equivalent SDoF system and its predictability for earthquake response. *J Struct Constr Eng*. 2001;**66**:75-85 (in Japanese).
16 Building Guidance Division of Hosing Bureau, Ministry of Land, Infrastructure, Transport and Tourism. Calculation examples and commentaries for the capacity spectrum method ver. 2001, Kougaku Tosyo, 2001 (in Japanese).
17 Engineering Affairs Division of Ministry of Construction and Japan Association for Building Research Promotion. *Guidelines for Evaluating the Seismic Capacity of Reinforced Concrete Buildings*. Tokyo: Gihodo Press; 2000 (in Japanese).
18 Shibata A. *Dynamic Analysis of Earthquake Resistant Structures*. Sendai: Tohoku University Press; 2010 (in Japanese).
19 Kashihara S. *Wavelet Beginner's Guide*. Tokyo: Tokyo Denki University Press; 1995 (in Japanese).
20 Hinata T, Kusunoki K, Tasai A, Kawamura M. An analytical study on the accuracy of the capacity curve derived from the measured acceleration for residual seismic capacity evaluation system with wavelet transformation. *Proc Jpn Concr Inst*. 2013;**35**:931-936 (in Japanese).
21 Masami O, Shinichi M, Koichi K, Yoshiaki N. Shaking table test of full-scale reinforced concrete three-story frame structure (part 1 object and outline of specimen). Summaries of Technical Papers of Annual Meeting Architectural Institute of Japan. C-2, Structures IV, 707-708, 1995 (in Japanese)
22 Tomoyoshi I, Akihiko N, Shigeyuki A, Fumitoshi K. Shaking table test of full-scale reinforced concrete three-story frame structure (part 2 outline of experiment). Summaries of Technical Papers of Annual Meeting Architectural Institute of Japan. C-2, Structures IV, 709-710, 1995 (in Japanese)
23 Isao K, Manabu T, Toshihiro H, Chikahiro M. Shaking table test of full-scale reinforced concrete three-story frame structure (part 3 results of experiments). Summaries of Technical Papers of Annual Meeting Architectural Institute of Japan. C-2, Structures IV, 711-712, 1995 (in Japanese)
24 Shigeyuki A, Keiji K, Hiroshi H, Hiroaki E. Shaking table test of full-scale reinforced concrete three-story frame structure (part 4 comparison between test and analytical results). Summaries of Technical Papers of Annual Meeting Architectural Institute of Japan. C-2 Structures IV, 713-714, 1995 (in Japanese)
25 National Institute for Earth Science and Disaster Resilience. Experimental study on the collapse mechanism of reinforced concrete structure under a severe seismic shaking, 1993 Annual Report, 1993 (in Japanese).

How to cite this article: Kusunoki K, Hinata D, Hattori Y, Tasai A. A new method for evaluating the real-time residual seismic capacity of existing structures using accelerometers: Structures with multiple degrees of freedom. *Jpn Archit Rev*. 2018;1:77–86. https://doi.org/10.1002/2475-8876.1010